

Supplemental Material

Comparison between Grating Imaging and Transient Grating Techniques on Measuring Carrier Diffusion in Semiconductor

Ke Chen¹, Xianghai Meng¹, Feng He^{1,2}, Yongjian Zhou¹, Jihoon Jeong¹, Nathaniel Sheehan³, Seth R Bank³, and Yaguo Wang^{1,2}*

1. Department of Mechanical Engineering, The University of Texas at Austin, Austin, TX, 78712, USA
2. Texas Materials Institute, The University of Texas at Austin, Austin, TX, 78712, USA
3. Department of Electrical and Computer Engineering, The University of Texas at Austin, Austin, TX, 78758, USA

*Corresponding Author. Email: yaguo.wang@austin.utexas.edu

1. Photoluminescence of the sample under test: a 30-periods GaAs(6nm)/AlAs(6nm) superlattice

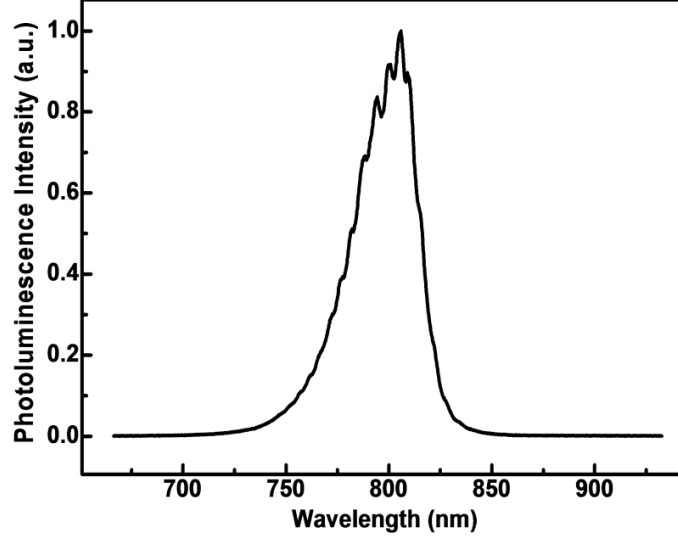


Figure s1. Photoluminescence of the sample under test: 30 periods of GaAs(6nm)/AlAs(6nm) super lattice

2. Analysis on the relative change of both the real and imaginary parts of refractive index induced by carrier excitation

Generally speaking, after a pump pulse generates excited carriers in a semiconductor, both the real part n and the imaginary part κ of the refractive index of the material will change, i.e. $n=n_0+\Delta n$, $\kappa=\kappa_0+\Delta\kappa$, which will result in a change in both reflectivity and transmittance, $R=R_0+\Delta R$, and $T=T_0+\Delta T$. However, the excited-carrier-induced changes in n and k and their importance will be different in different detection regions. In the following analysis, we will show that in resonant detection region where the probe photon energy is close to the bandgap of the material, $\Delta\kappa/\kappa_0$ (the absorption change) is typically much larger than $\Delta n/n_0$ (the phase change); but at probe wavelengths far away from resonance, $\Delta\kappa/\kappa_0$ is usually negligible while $\Delta n/n_0$ will dominate.

In a real physical system, the $\Delta n/n_0$ and $\Delta\kappa/\kappa_0$ are not independent parameters, but correlated to each other through the Kramers-Kronig relation, which is expressed as:

$$n(\omega) = 1 + \frac{2}{\pi} P \int_0^{\infty} \frac{\omega' \kappa(\omega')}{\omega'^2 - \omega^2} d\omega', \quad (s1)$$

$$\kappa(\omega) = \frac{2\omega}{\pi} P \int_0^{\infty} \frac{n(\omega') - 1}{\omega'^2 - \omega^2} d\omega', \quad (s2)$$

Hence, the change of the real and imaginary parts of refractive index are also correlated:

$$\Delta n(\omega) = \frac{2}{\pi} P \int_0^{\infty} \frac{\omega' \Delta \kappa(\omega')}{\omega'^2 - \omega^2} d\omega', \quad (\text{s3})$$

$$\Delta \kappa(\omega) = \frac{2\omega}{\pi} P \int_0^{\infty} \frac{\Delta n(\omega')}{\omega'^2 - \omega^2} d\omega', \quad (\text{s4})$$

If the magnitude of either n change or κ change is known, we can use Equations (s3)~(s4) to estimate the change of the other one. In a semiconductor structure with well-defined band structure, such as GaAs/AlAs super lattice in our case, the excited carrier induced absorption change ($\Delta\kappa$) is typically due to the phase space filling effect. After carrier thermalization and cooling, the excited carriers will mainly occupy the band edge energy states (or the exciton state for 2D or low temperature cases), giving rise to an absorption change **only non-trivial at around band edge** (or the exciton energy).^[1-4] Since photoluminescence (PL) signal can just reflect the distribution of the excited carriers at the band edge, the absorption change $-\Delta\kappa(\omega)$ and the PL signal typically will have the same shape.^[1,5] Based on this understanding, we can assume the absorption change with the following expression:

$$\Delta \kappa(\omega) = -A(\omega) \exp(-4 \ln 2 \frac{(\omega - \omega_g)^2}{\Gamma^2}) \kappa_0(\omega), \quad (\text{s5})$$

where $\kappa_0(\omega)$ is the extinction coefficient before excitation, which has been measured and modeled in references,^[6,7] ω_g is the angular frequency corresponding to the band gap of the direct transition, and Γ is a line width parameter characterizing the occupied energy range, and $A(\omega)$ is the absorption reduced ratio with a step-function like shape (to eliminate the part with energies lower than the direct band gap where little is contributed to the absorption change). The profile of carrier induced absorption change $\Delta\kappa(\omega)/\kappa_0$ based on equation (s5) is plotted in Figure s2 as the black curve. By substituting Equation (s5) into Equation (s3), we can calculate the correlated change of real part of refractive index, $\Delta n/n_0$, which is also plotted in Figure s2. It can be seen that, in the resonant region (marked by green dashed rectangle), $\Delta\kappa/\kappa_0$ is much larger than $\Delta n/n_0$, showing at the band edge states, the excited carriers have much greater influence on the extinction coefficient (absorption) than on the real refractive index. In the non-resonant regions (marked by blue dashed rectangles), $\Delta\kappa/\kappa_0$ is negligible but $\Delta n/n_0$ is non-trivial, showing the excited carriers mainly cause change in the real part of refractive index in these regions. Physically, the dominant change in $\Delta\kappa/\kappa_0$ at the band edge states comes from the phase-space filling (Pauli blocking effect). Because $\frac{1}{\omega'^2 - \omega^2}$ in

equation (s3) has odd symmetry with respect to ω and vanishes away from ω , and the integrand in equation (s3) at the band edge ω is a product of the odd symmetric term with a smooth and gradual change term $\omega' \Delta\kappa(\omega')$, hence, in the resonant region, this integrand will have opposite sign with comparable magnitude, which will result in a major cancellation when performing the integration to get the refractive index change $\Delta n(\omega)$. So mathematically it is reasonable to reach a small $\Delta n(\omega)$ around the band edge ω .

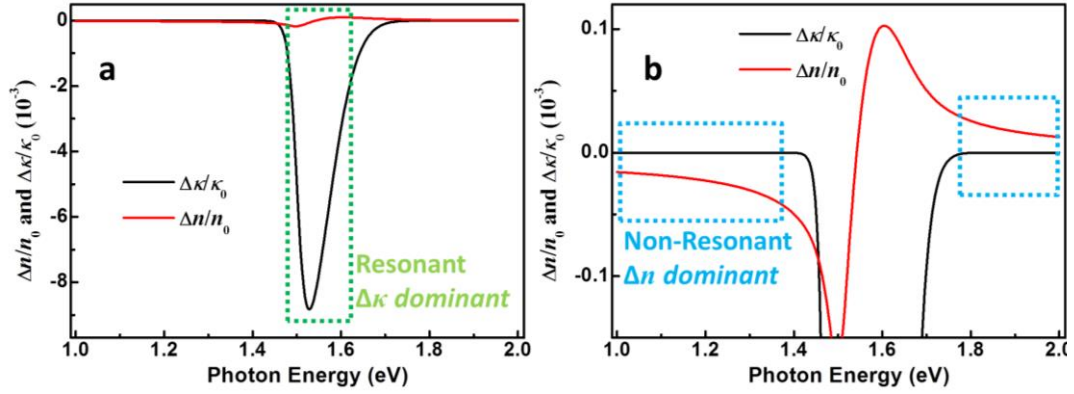


Figure s2. The excited-carrier-induced refractive index change in GaAs/AlAs superlattice calculated from Kramers-Kronig relation. (a) In the resonant region (circled by green dashed rectangle), $\Delta\kappa/\kappa_0$ is much larger than $\Delta n/n_0$; (b) while in the non-resonant region (circled by blue dashed rectangles), $\Delta\kappa/\kappa_0$ is almost 0 but $\Delta n/n_0$ is non-trivial.

In our experiment, the probe wavelength is 800 nm with the photon energy close to the band gap (1.53 eV, see Figure s1). Therefore, the assumption made in the model derivation in the manuscript that the carrier grating mainly modulates the imaginary part of the refractive index is valid for the probe laser.

3. Superlattice Sample Growth and Structure Characterization

Superlattice samples were grown on (001)-oriented, semi-insulating (undoped) GaAs substrates by solid-source molecular beam epitaxy (MBE) in an EPI Mod Gen. II system. GaAs and AlAs layers were grown at ~ 600 °C and at 2.0 Å/s with an As_2 /group-III beam, with equivalent pressure (BEP) ratio of 15 (As_2 /group-III flux ratio of ~ 1.9) and 3.5×10^{-6} Torr BEP of As_2 for GaAs, and an As_2 /group-III beam equivalent pressure (BEP) ratio of 22 and 2.4×10^{-6} Torr BEP of As_2 for AlAs. The group-III cell temperatures and BEPs were held constant throughout the growth of the structures, and the As_2 cracker cell valve position and BEP were varied depending on the material being grown. The structure consists of a GaAs buffer layer, AlAs lateral etch release layer, GaAs pre-superlattice layer, and a GaAs on AlAs superlattice consisting of 30-periods of 6nm of each material, starting with 6nm of AlAs on the pre-superlattice layer and ending with 6nm GaAs on top of the epitaxial layer stack. Growth rates were calibrated with reflection high-energy electron-diffraction (RHEED) intensity oscillation measurements, where one atomic layer corresponds to one period of the intensity oscillations. It is important to note that this technique is sensitive to growth rate transients associated with shuttering, though these are negligible with modern dual zone SUMO sources (the change in reflected heat is minimal upon shuttering due to the small apertures). Superlattices (SLs) were grown based upon these calibrated with ω -2 θ XRD scans, and fitted with dynamical scattering methods (designed based on the RHEED calibrations) to

extract the thicknesses. Fig. s3 shows two illustrative plots of the experimental data for the sample we measured: 30 period 6/6 nm GaAs/AlAs SLs. Additional simulations were undertaken to determine the deviation of the actual structures from the nominal layer structures — as expected, minimal deviation was observed. Simulations of both samples show close agreement with the measured XRD data. As stated, the samples were fitted with dynamical scattering methods to extract the thicknesses. This method gives the average thickness of each constituent period for the grown structure. The three center peaks of each sample are: (from right to left) the GaAs substrate peak, the QW structure peak, and the AlAs layer that was grown between the GaAs buffer layer and the QW structure. Using the fitting, it has been determined that the 6/6 nm (12 nm per period) sample is 6.0/5.9 nm GaAs/AlAs (12 nm per period, using two significant figures).

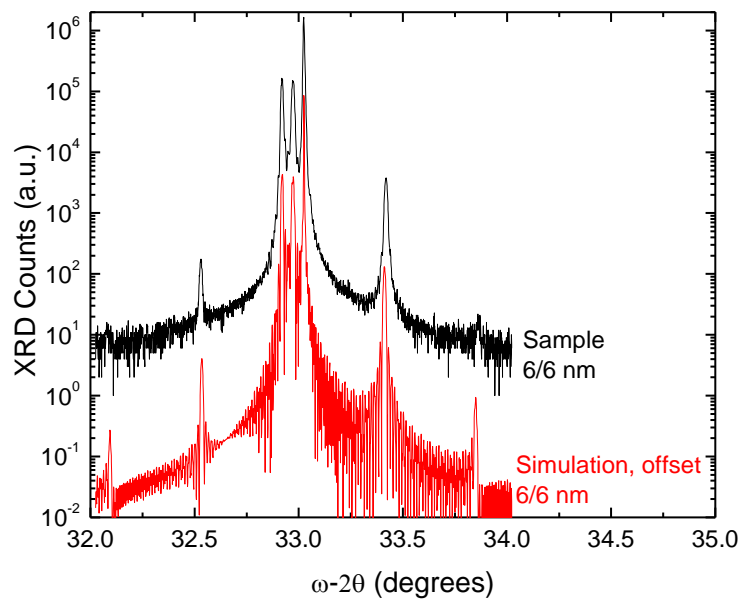


Fig. s3. Measured and simulated XRD data of the sample measured: 30 periods 6nmGaAs/6nmAlAs

4. Checking the linear relation between the signal amplitude and the pump fluence

We have tested this linearity with grating imaging technique, using 3 pump beams and 3 probe beams (case 1). The results are shown below in Fig. s4, where we can see that the amplitudes of the signals measured at two pump fluences also increases linearly with the pump fluence (Normalized signal curves overlap and signal amplitude scales with pump power). This further validates the assumption that the local transmission change is proportional to the local carrier density. Using Eq. (1) in the manuscript, we fitted the signals and obtained two close diffusion coefficients, which is reasonable, because in the linear region the diffusion coefficient is supposed to be independent of the pump power.

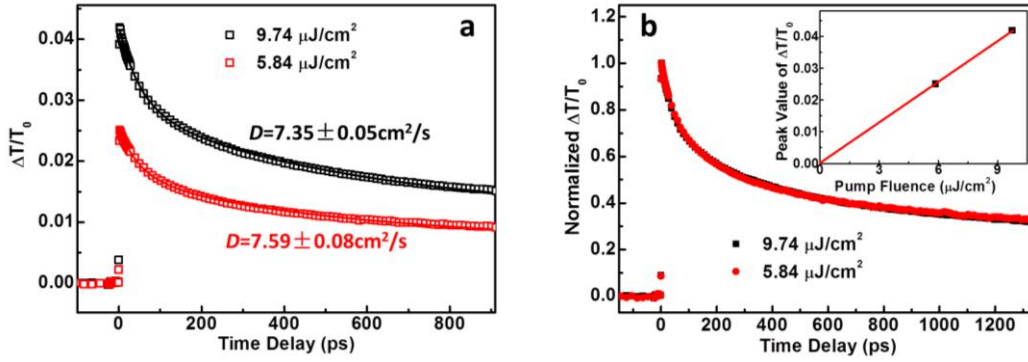


Fig. s4. (a) Differential transmission signal measured with grating imaging technique at two different pump fluences. The solid lines are the fitting curves using Equ. (1) in the manuscript. (b) Normalized differential transmission signals. Inset: Peak values of the signals shown in figure (a).

5. Estimation of the laser spot size

The spot size of pump and probe are obtained by an imaging system. In our setup, we utilized the objective lens to form the image of the grating onto the sample surface, we also utilized the same objective lens plus a flipping mirror and a CCD camera to compose an imaging system to observe the sample surface and the grating-modulated laser spots on it as well. The image of the pump and probe spots on the sample are shown in Fig. s5. Bright and dark fringes can be seen clearly for both pump and probe spots, which are modulated by the transmission grating with the same pattern. A bright fringe passes through two markers for both spots, indicating a very good overlap between pump and probe fringes. Since the period of the transmission grating and the imaging ratio of the objective lens are already known (80 μm and 20X), the period of the grating image on the surface is just $80\mu\text{m}/20=4\mu\text{m}$. Therefore, we can estimate the laser spot size by directly counting the number of period that the laser spot covers. By this means, the estimated pump and probe spot sizes are 70 μm and 35 μm , respectively. Note that we use a lens before the transmission grating to reduce laser beam sizes on the grating surface and on the objective lens aperture as well, so actually the laser beam is convergently (with oblique angles) incident onto the objective lens, which results in a relatively larger spot size than the collimate incident case.

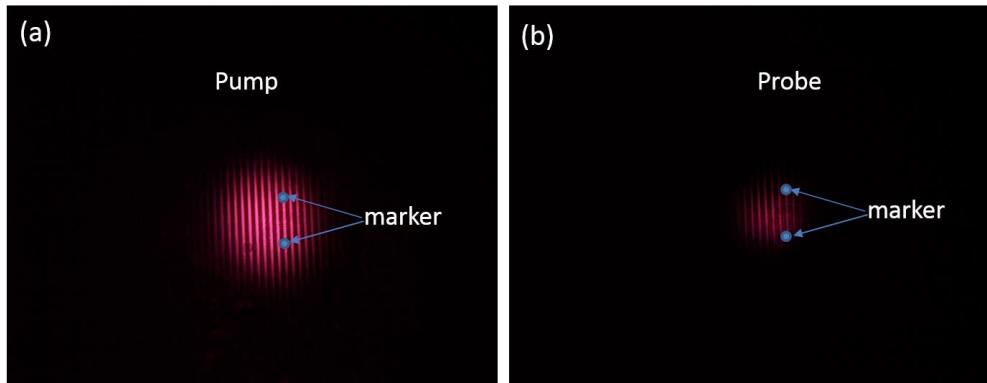


Fig. s5. Images of (a) pump and (b) probe spots on sample surface taken by an CCD camera monitoring the sample surface in the experimental setup. A bright fringe passes through two markers for both spots, indicating a very good overlap between pump and probe fringes.

6. Estimation of the excited carrier density

To calculate the excited carrier density, one information we need is the light absorption. This quantity can be acquired by transfer matrix method, as documented in Ref. [8]. The main idea is to calculate the reflectance on the sample surface and the transmittance into the substrate. Using energy conservation law, the absorption is estimated as: $Absorptance = 1 - Reflectance - Transmittance$. With this method, the calculated absorption of the superlattice is $1 - 0.0939 - 0.6476 = 0.2585$. So, the estimated carrier density corresponding to $9.74 \mu\text{J}/\text{cm}^2$ (the maximum pump fluence we used) is $5.64 \times 10^{17}/\text{cm}^3$. This value is well below the theoretical saturation density, $3.67 \times 10^{18}/\text{cm}^3$, estimated from the density of states and the thickness of quantum well, along with the bandwidth of the laser pulse^[8]. The validity of the small excitation and thus the linearity assumption is again demonstrated.

7. Error analysis

The errors shown in Table 1 of maintext are the standard error of the fitted parameter (diffusion coefficient D here) from the fitting procedure with Origin software. The formula of how to calculate the errors can be found in OriginalLab Origin Help book^[9]. These errors can represent the precision of the fitted parameters. As a reliable fitted result, the magnitude of the standard error should be much lower than the fitted value, like in our cases. If the error is larger than the fitted value, it indicates the fitted result is not reliable or the fitting model is over-parameterized. Seemingly the standard error of D does not manifest the noise level, which could be that the fitting models are different. In case 5 of Fig. 2 in the maintext, the key term in the model is $\exp(-2f^2Dt)$, while in other cases the key term is $\exp(-f^2Dt)$. Therefore, the same amount of error in D could result in more noise in case 5. Since standard error is more associated with the precision of the fitting parameter but not the noise level, it's not recommended to compare standard errors between two models to check the noise. To

manifest the noise level, the root mean squared error (RMSE), which represents how far the data points scatter away from its expected value (the fitting curve), is more relevant. RMSE of all cases have been added Table S1, as shown below. It can be seen that in case 5 where the experimental signal is much noisier than other cases, the RMSE value is indeed much larger.

Table S1. The fitted carrier diffusion coefficients for different cases. The deviations are standard error (SE) obtained from the fitting process. RMSE is the root mean squared error, reflecting the noise level of experimental data

	Case 1	Case 2	Case 3	Case 4	Case 5
$D \pm SE$ (cm ² /s)	7.35 \pm 0.05	7.45 \pm 0.4	7.42 \pm 0.5	7.46 \pm 0.1	6.95 \pm 0.4
RMSE	0.00414	0.0131	0.0219	0.00824	0.0568

References:

- (1) Sun, D.; Rao, Y.; Reider, G. A.; Chen, G.; You, Y.; Brézin, L.; Harutyunyan, A. R.; Heinz, T. F. Observation of rapid exciton–exciton annihilation in monolayer molybdenum disulfide. *Nano Lett.* **2014**, *14* (10), 5625-5629.
- (2) Bennett, B. R.; Soref, R. A.; Del Alamo, J. A. Carrier-induced change in refractive index of InP, GaAs and InGaAsP. *IEEE J. Quantum Electron.* **1990**, *26* (1), 113-122.
- (3) Wang, Y.-T.; Luo, C.-W.; Yabushita, A.; Wu, K.-H.; Kobayashi, T.; Chen, C.-H.; Li, L.-J. Ultrafast multi-level logic gates with spin-valley coupled polarization anisotropy in monolayer MoS₂. *Sci. Rep.* **2015**, *5*.
- (4) Steinhoff, A.; Rosner, M.; Jahnke, F.; Wehling, T.; Gies, C. Influence of excited carriers on the optical and electronic properties of MoS₂. *Nano Lett.* **2014**, *14* (7), 3743-3748.
- (5) Kumar, N.; Cui, Q.; Ceballos, F.; He, D.; Wang, Y.; Zhao, H. Exciton-exciton annihilation in MoSe₂ monolayers. *Phys. Rev. B* **2014**, *89* (12), 125427.
- (6) Aspnes, D. E.; Kelso, S. M.; Logn, R. A.; Bhat, R. Optical properties of Al_xGa_{1-x}As. *Journal of Applied Physics* **1986**, *60*, 754
- (7) Adachi, S. Optical dispersion relations for GaP, GaAs, GaSb, InP, InAs, InSb, Al_xGa_{1-x}As and In_{1-x}Ga_xAs_yP_{1-y}. *Journal of Applied Physics* **1989**, *66*, 6030
- (8) Chen, K. et al, Measurement of ambipolar diffusion coefficient of photoexcited carriers with ultrafast reflective grating-imaging technique, *ACS Photonics*, vol. 4, no. 6, pp. 1440-1446, **2017**
- (9) https://www.originlab.com/doc/Origin-Help/Interpret-Regression-Result#Standard_Error